

77. Savin AV, Sakovich RA, Mazo MA. Using spiral chain models for study of nanoscroll structures. *Physical Review B*. 2018;97(16):165436. DOI:10.1103/PhysRevB.97.165436

78. Kulagin AE, Shapovalov AV. Analytical description of the diffusion in a cellular automaton with the Margolus neighbourhood in terms of the two-dimensional Markov chain. *Mathematics*. 2023;11(3):584. DOI:10.3390/math11030584

79. Bukharov DN, Skryabin IO, Arakelyan SM. Model of the microscroll structure. *Journal of Physics: Conference Series*. 2019;1331(1):012019. DOI:10.1088/1742-6596/1331/1/012019

80. Burlakov RB, Kovivchak VS. On the issue of measuring the resistivity of conductive layers using the four-probe method. *Vestnik Omskogo Universiteta*. 2014;2(72):59-68. (In Russ.)

81. Apostolova T, Kurylo V, Gnilitzkiy I. Ultrafast laser processing of diamond materials: A Review. *Frontiers in Physics*. 2021;9:650280. DOI:10.3389/fphy.2021.650280

82. Tikhomirov S, Kimstach T. Raman spectroscopy – a promising method for studying carbon nanomaterials. *Analitika*. 2011;(6):28-32. (In Russ.)

83. Shimizu M, Shimotsuna Y, Sakakura M, Yuasa T, et al. Periodic metallo-dielectric structure in diamond. *Optics Express*. 2009;17(1):46-54. DOI:10.1364/OE.17.000046

84. Kononenko TV, Komlenok MS, Pashinin VP, Pimenov SM, et al. Femtosecond laser microstructuring in the bulk of diamond. *Diamond and Related Materials*. 2009;18(2-3):196-199. DOI:10.1016/j.diamond.2008.07.014

85. Kononenko TV, Konov VI, Pimenov SM, Rossukanyi NM, et al. Three-dimensional laser writing in diamond bulk. *Diamond and Related Materials*. 2011;20(2):264-268. DOI:10.1016/j.diamond.2010.12.013

86. Sun B, Salter PS, Booth MJ. High conductivity micro-wires in diamond following arbitrary paths. *Applied Physics Letters*. 2014;105(23):231105. DOI:10.1063/1.4902998

87. Shimotsuna Y. Three-dimensional nanostructuring of transparent materials by the femtosecond laser irradiation. *Journal of Laser Micro/Nanoengineering*. 2006;1(3):181-184. DOI:10.2961/jlmn.2006.03.0006

88. Lagomarsino S, Bellini M, Corsi C, Fanetti S, et al. Electrical and Raman-imaging characterization of laser-made electrodes for 3D diamond detectors. *Diamond and Related Materials*. 2014;43:23-28. DOI:10.1016/j.diamond.2014.01.002

89. Kulnitsky BA, Perezhogin IA, Blank VD. Polytypes and twins in the diamond – lonsdaleite system. *Izvestiya vysshikh uchebnykh zavedeniy. Seriya Khimiya i khimicheskaya tekhnologiya = ChemChemTech*. 2015;5(58):48-50. (In Russ.)

90. Ying P, Gao Y, Zhang B, Wu Y, et al. Synthesis of twin-structured nanodiamond particles. *AIP Advances*. 2020;10(1):015240. DOI:10.1063/1.5141035

Different DLA calculation schemes with Moore and/or von Neumann Neighborhoods

P.1. Algorithm for fiber model construction

The algorithm for constructing the fiber model in the DLA approach was developed from the following steps (Fig. P.1): (1) At the initialization stage, a starting structure consisting of a system of seed particles located on the lower boundary was generated within the calculation area with a uniform grid, and the fiber size (maximum number of particles in the calculation area) was set; (2) A specified number of particles were generated at the upper boundary of the calculation area; (3) These particles performed random shifts downward and sideways with equal or different probabilities; (4) If they approached an occupied cell within the Moore neighborhood (Fig. P.1b), they aggregated with the occupied cell; otherwise, they continued moving; (5) Steps 2-4 were repeated.

The criterion for stopping the iterative process was the fiber reaching the required size, when the number of particles in the calculation area reached the set value, or when the nanowire reached the upper boundary of the calculation area.

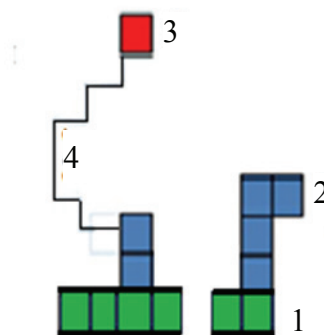


Fig. P.1a. DLA fiber model calculation scheme: 1 – starting structure, 2 – aggregated particles, 3 – new particle, 4 – random shifts. Explanations are provided in the text

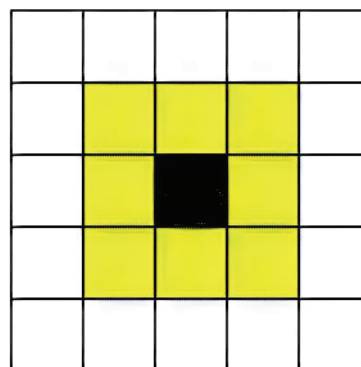


Fig. P.1b. Moore neighborhood of 8 objects

P.2. Two models of growth over inhomogeneity – random growth during particle deposition in percolation

To describe the algorithm, two functions are used: the average surface height $\overline{h(t)}$, which defines the baseline position for the surface of the sample being studied, and its roughness, $W(t)$.

In the first random growth model, all growth columns are filled randomly (Fig. P.2a). Then, after the random deposition of N particles, the height of the deposited structure h can be calculated using the equation:

$$h = \sqrt{Nf(1-f) + (Nf)^2},$$

where $f = 1/L$ is the probability of filling a given column, and L is the width of the calculation area, i.e., $h^i = h^{i-1} + 1$, where i is the time step [68].

In the other model of ballistic percolation deposition, a particle is fixed at the point of first contact with the already deposited structure, following the nearest neighbor rule (Fig. P.2b). In this case, the height is determined by the heights of the nearest left and right columns, and the height is calculated as the maximum of the neighboring columns' heights:

$$h_j = \max\{h_{j-1}, h_j + 1, h_{j+1}\},$$

where j is the number of the column being considered [69]. Unlike the previous model (Fig. P.2a), in this case, the particle can attach to the side surface of the already formed structure (Fig. P.2a) [70]. This means that the possibility of growth along the local normal to the surface is considered, which can lead to the expansion of local protrusions on the growth front surface, thus enhancing surface growth in the lateral direction.

The percolation structure is represented as a square grid of size $m \times m$ a. u. The cells of this grid contain either 0 (empty site) or 1 (occupied site). Each cell in the model is occupied by a particle with probability s , independent of the state of neighboring cells. For each grid cell, a random number α is generated. If $\alpha \leq s$, the value in the cell is set to 1; otherwise, it is 0 (cf. with [71]). Here, the parameter s represents the percolation threshold, above which a particle is not fixed in the cell.

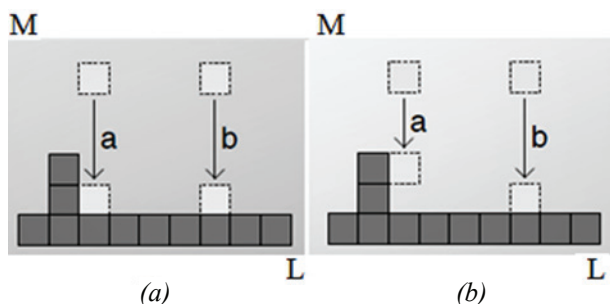


Fig. P.2. Diagram of both (a) Random and (b) Ballistic the deposition processes for Deposited Particles – also, the moving particles labeled as letters both a and b

P.3. DLA model in the iterative algorithm

The initial state of the system was described by placing model particles, such as Au particles, along the lower boundary, serving as aggregation centers. Each iteration began by introducing a new model particle into the calculation area. The particle was introduced at a random location along the upper boundary, within its central third. This simulates the experiment where a laser beam with a diameter of $1/3$ of the calculation area length is applied. Then, the standard DLA procedure was followed (Fig. P.3).

The random walk of the particle occurred from the upper boundary of the calculation area, where a notional cathode was located, to the lower boundary, where a notional anode was located. If an occupied area appeared in the Moore neighborhood of the wandering particle, it would aggregate with that area with a given probability.

To describe the random walk, a uniform grid was applied to the calculation area. Thus, the random walk was formed by a series of single-cell movements across the calculation area with a specified probability. Periodic boundary conditions were used along the sides, causing the particle to reflect off them. At the lower boundary, an adhesion condition was applied, fixing the particle in place. Varying the probabilities of individual random movements allowed for consideration of growth direction. Aggregation of the wandering particle occurred with a given probability when it encountered an occupied cell in the Moore neighborhood. In terms of physics, the aggregation probability can be understood as a conditional surface tension coefficient in the system, inversely proportional to temperature, normalized to the phase transition temperature [73].

To model experimental samples, a random nanowire model was proposed [74], where a system of random lines of equal thickness was generated on a two-dimensional calculation area. Each line was assigned a random length L from the interval $[L_{\min}; L_{\max}]$; the area had a width w . A line was defined by two points (x_1, y_1) and (x_2, y_2) with random coordinates as follows:

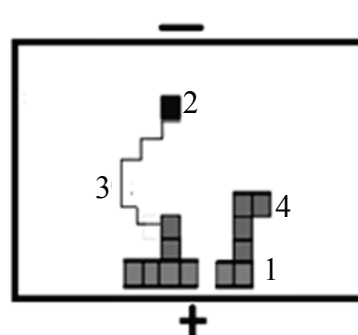


Fig. P.3. Model Diagram (One Iteration of the DLA Process):
 1 – Au particles, 2 – C chain, 3 – its random walk,
 4 – previously formed structure.
 The signs (+) and (–) correspond to the direction of the applied external electric field

$$\begin{aligned}
 x_c &= rw; & y_c &= rL; & \theta &= 2\pi r; \\
 x_2 &= x_c + L\cos(\theta)/2; & y_2 &= y_c + L\sin(\theta)/2; \\
 x_1 &= x_c - L\cos(\theta)/2; & y_1 &= y_c - L\sin(\theta)/2,
 \end{aligned}$$

where r is a random number with a uniform distribution, and θ is the angle of rotation of the wire segment.

P.4. Model for an individual microsp sponge

Figure P.4 presents calculations based on the proposed model: laser radiation was assumed to act on the lower boundary, where the anode (charge (+)) was located. Objects of different sizes were generated, moving with a given speed toward the upper boundary, where the cathode (charge (-)) was located.

The calculation area was conventionally divided into three subregions: two with a side length of 33 a. u., and the uppermost one with a length of 34 relative units. In these areas, the object movement speeds decreased to 3 a. u., 2 a. u., and 1 relative a. u., respectively. The probability of object merging was 20 %. The sizes of the model objects

varied from 1 to 5 a. u. For example, Fig. P.4a shows the case of forming a sponge from small elements; Fig. P.4b illustrates the formation of individual elongated threads; in Fig. P.4c, several small sponges are generated; and in Fig. P.4d, most objects have merged into one large elongated sponge.

P.5. Helicoidal structure model

The diffusion model of a helicoidal structure was based on solving the diffusion equation in a discrete area using cellular automaton techniques [78]. The structure was synthesized iteratively, starting from an initial shape, where a cell in the calculation area would become occupied with a given probability if it had a neighboring occupied cell within the Moore neighborhood (considering 8 adjacent cells, as shown in Fig. P.5). The main parameter of the model was the probability of a cell being occupied. This relative model parameter can be related to a physical parameter of the system, such as the intensity of an external magnetic field in the corresponding experimental geometry.

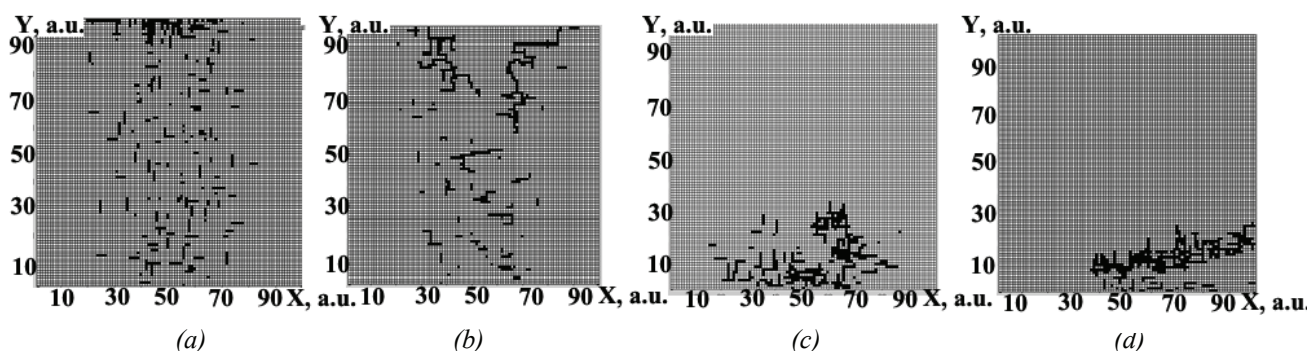


Fig. P.4. Model of a sponge system made from individual threads (in the horizontal plane relative to the boundary): a system of small sponges made of short threads, located near the upper boundary of the calculation area (a); a system of vertically elongated sponges, made of individual long threads, localized near the upper boundary of the calculation area (b); a system of small sponges with a relatively uniform structure, localized near the lower boundary of the calculation area (c); a system of sponges made from one large elongated object, located near the lower boundary of the calculation area (d)

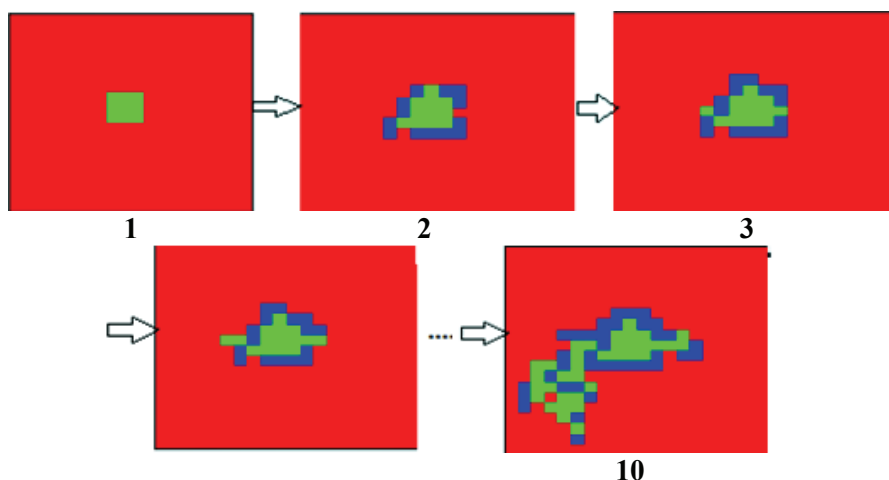


Fig. P.5. Model diagram: the resulting helical structure after performing 1–10 iterations, starting from the initial shape numbered 1 (explanations are provided in the text).